Science of the Total Environment 849 (2022) 157626

Contents lists available at ScienceDirect

Science of the Total Environment

journal homepage: www.elsevier.com/locate/scitotenv

Exploring GHG emissions in the mainstream SCEPPHAR configuration during wastewater resource recovery

Borja Solís [a], Albert Guisasola [a,*], Maite Pijuan [b,c], Juan Antonio Baeza [a]

[a] GENOCOV, Departament d'Enginyeria Química, Biològica i Ambiental, Escola d'Enginyeria, Universitat Autònoma de Barcelona, 08193 Bellaterra, Barcelona, Spain
[b] Catalan Institute for Water Research (ICRA), Emili Grahit 101, 17003 Girona, Spain
[c] University of Girona, Girona, Spain

HIGHLIGHTS

- Long-term assessment of GHG emissions from the mainstream SCEPPHAR configuration
- Low GHG emissions even with high nitrite accumulation.
- Low DO set-points led to lower emissions by hindering N_2O transfer to the gas phase.
- A peak of N_2O emission was found attributed to the transient conditions of AOB.
- The intermittent aeration strategy mitigated N_2O emissions by 40 %.

GRAPHICAL ABSTRACT

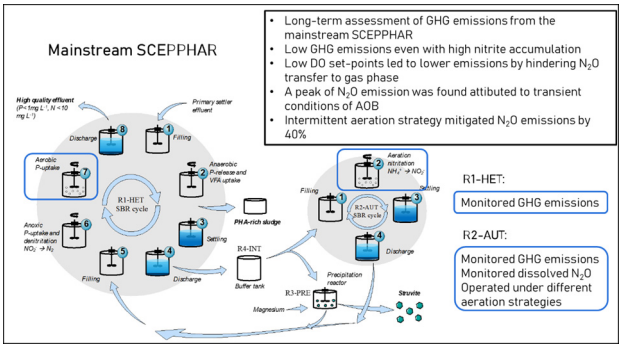

ARTICLE INFO

Editor: Paola Verlicchi

Keywords:
Enhanced biological phosphorus removal (EBPR)
GHG mitigation
Greenhouse gases (GHG)
Pilot plant
Water resource recovery facility (WRRF)

ABSTRACT

The wastewater sector paradigm is shifting from wastewater treatment to resource recovery. In addition, concerns regarding sustainability during the operation have increased. In this sense, many water utilities have become aware of the potential GHG emissions during the operation of wastewater treatment. This study assesses the nitrous oxide and methane emissions during the long-term operation of a novel wastewater resource recovery facility (WRRF) configuration: the mainstream SCEPPHAR. The long-term N_2O and CH_4 emission factors calculated were in the low range of the literature, 1 % and 0.1 %, respectively, even with high nitrite accumulation in the case of N_2O. The dynamics and possible sources of production of these emissions are discussed. Finally, different aeration strategies were implemented to study the impact on the N_2O emissions in the nitrifying reactor. Results showed that operating the pilot-plant under different dissolved oxygen concentrations (between 1 and 3 g O_2 m^{-3}) did not have an effect on the N_2O emission factor. Intermittent aeration was the aeration strategy that most mitigated the N_2O emissions in the nitrifying reactor, obtaining a reduction of 40 % compared to the normal operation of the pilot plant.

1. Introduction

Over the past years, the scarcity of natural resources and the concern for sustainability, with particular emphasis on climate change due to greenhouse gas (GHG) emissions, have shifted the wastewater sector paradigm towards a resource recovery scenario. Therefore, wastewater treatment plants (WWTPs) are being transformed into water resource recovery facilities (WRRFs). The objective of these facilities is not only to achieve a good effluent quality under the constraints of technical feasibility and cost but also to recover resources (bioplastics, cellulose or nitrogen (N), and phosphorus (P) into fertilizers such as struvite), water or energy (in energy carriers such as methane (CH_4) or hydrogen) in a sustainable way. Novel WRRFs configurations as well as innovative operational and control strategies have arisen recently to promote this new paradigm shift.

* Corresponding author.
E-mail addresses: Borja.Solis@uab.cat (B. Solís), Albert.Guisasola@uab.cat (A. Guisasola), mpijuan@icra.cat (M. Pijuan), JuanAntonio.Baeza@uab.cat (J.A. Baeza).

http://dx.doi.org/10.1016/j.scitotenv.2022.157626
Received 20 May 2022; Received in revised form 19 July 2022; Accepted 21 July 2022
Available online 25 July 2022

Abbreviations

AOB	Ammonia oxidizing bacteria
AOR	Ammonia oxidation rate
C	Carbon
CH_4	Methane
CH_4-EF	Methane emission factor
CO_2	Carbon dioxide
COD	Chemical oxygen demand
COD_S	Soluble chemical oxygen demand
COD_T	Total chemical oxygen demand
DO	Dissolved oxygen
DO_{SP}	Dissolved oxygen set point
DPAO	Denitrifying polyphosphate accumulating organisms
EBPR	Enhanced biological phosphorus removal
GHG	Greenhouse gas
Mg^{2+}	Magnesium ion
$MgCl_2$	Magnesium chloride
N	Nitrogen
N_2	Nitrogen gas
N_2O	Nitrous oxide
N_2O-EF	Nitrous oxide emission factor
NH_2OH	Hydroxylamine
NH_4^+	Ammonium
NO	Nitric oxide
NO_2^-	Nitrite
NO_3^-	Nitrate
NOB	Nitrite oxidizing bacteria
ORP	Oxidation-reduction potential
P	Phosphorus
PAO	Polyphosphate accumulating organisms
PHA	Poly-hydroxyalkanoate
PO_4^{3-}	Phosphate
R1-HET	Heterotrophic reactor
R2-AUT	Autotrophic reactor
R3-PRE	Precipitation reactor
R4-INT	Interchange reactor
SBR	Sequencing batch reactor
SCEPPHAR	Short-cut enhanced phosphorus and PHA recovery configuration
SP	Set point
SRT	Sludge retention time
SI	Supplementary information
TN	Total nitrogen
TSS	Total suspended solids
V	Volume
VFA	Volatile fatty acid
VSS	Volatile suspended solids
WRRF	Water resource recovery facility
WWTP	Wastewater treatment plant

Regarding resource recovery, P arises as a perfect candidate for its recovery from wastewater. P is essential for our society in the production of fertilizers. However, the main source of P is the phosphate rock and it is estimated to be depleted in the next 50–300 years (Cieślik and Konieczka, 2017; Cordell et al., 2011). During wastewater treatment, it is estimated that 3 million tons of P are removed yearly, showing that the implementation of P-recovery strategies would mitigate the current dependency on phosphate rocks (Mayer et al., 2016). Biological P removal during wastewater treatment is based on promoting the growth of polyphosphate accumulating organisms (PAO) during the enhanced biological phosphorus removal (EBPR) process.

Regarding GHG emissions, nitrous oxide (N_2O) is produced and emitted during biological N removal on WRRFs through nitrification and denitrification (Kampschreur et al., 2009; Massara et al., 2017). N_2O is a potent GHG with a global warming potential 265 times higher than that of carbon dioxide (CO_2) (IPCC, 2014), therefore, the carbon (C) footprint of WRRF is highly sensitive to N_2O emissions. N_2O can be produced during biological oxidation of ammonium to nitrite via two pathways: i) the incomplete NH_2OH oxidation pathway, and ii) the nitrifier denitrification pathway (Kampschreur et al., 2009;Wunderlin et al., 2012; Chen et al., 2020). The parameters contributing the most to the activation of these pathways are: low dissolved oxygen (DO) levels, NO_2^- accumulation, ammonia oxidation rate (AOR) and transient conditions from low to high activity (Law et al., 2012; Massara et al., 2017; Vasilaki et al., 2019). During denitrification, N_2O is produced as an intermediate of the four step reduction reactions from NO_3^- to NO_2^-, nitric oxide (NO), N_2O and finally to nitrogen gas (N_2). In most wastewater treatment systems, the N_2O reducing capacity exceeds the capacity of producing N_2O, and therefore denitrification is often considered as an N_2O sink (Conthe et al., 2019). However, under certain conditions, N_2O can also accumulate during denitrification. The parameter that most affects N_2O accumulation during denitrification is the low chemical oxygen demand (COD) to N ratio (COD/N ratio) (Law et al., 2012).

CH_4 is also a GHG that is emitted during wastewater treatment. CH_4 is the second most important GHG after CO_2 and has a global warming potential 21 times higher than that of CO_2 (IPCC, 2014). Previous studies have demonstrated that CH_4 emitted during wastewater treatment can be present in the influent of the WRRF, produced under the anaerobic environments in the sewer network (Guisasola et al., 2008; Gutierrez et al., 2014; Mannina et al., 2018) or present in the reject water recirculated from the anaerobic digester (Ribera-Guardia et al., 2019; Rodriguez-Caballero et al., 2014).

The novel mainstream SCEPPHAR (Short Cut Enhanced Phosphorus and PHA recovery) configuration of WRRF has demonstrated at demo scale and under real influent conditions the feasibility of implementing resource recovery in the mainstream line (struvite and PHA-rich sludge) (Larriba et al., 2020). The mainstream SCEPPHAR is one of the novel technologies involved in the SMART-Plant project (www.smart-plant.eu). The whole project aimed to prove the feasibility of novel wastewater treatment technologies at pilot-scale towards a circular economy scenario. The mainstream SCEPPHAR pilot plant contains three sequencing batch reactors (SBR), the first mainly heterotrophic (R1-HET), designed to promote EBPR, the second reactor mainly autotrophic (R2-AUT) and a third one that acts as an interchange vessel. During the first long term operation of the mainstream SCEPPHAR, the pilot plant achieved successful removal efficiencies for C, P and N under nitrite shortcut N-removal, i.e. the N-removal via nitritation (NH_4^+ to NO_2^-) and denitritation (NO_2^- to N_2). The advantages of the nitrite pathway approach are the lower oxygen requirements for N oxidation, the lower COD requirements for denitrification processes and faster denitrification rate (Mavinic and Turk, 1987). However, nitrite accumulation can have a negative effect on the N_2O emissions (Law et al., 2012). Regarding nutrient recovery results, up to 45–63 % of the influent P load could be recovered as struvite in a separate reactor in the mainstream line (Larriba et al., 2020), which is higher than the 12 % of influent P reported within side-stream P-recovery (Remy and Jossa, 2015).

Therefore, the aim of this work was to monitor the long-term operation of the mainstream SCEPPHAR pilot plant, under real conditions and under nitrite shortcut N-removal in view of assessing the overall GHG emissions and the dynamics of these emissions through different pilot plant cycles. Different aeration strategies were implemented to critically assess its effect on the N_2O liquid concentration and emissions. Different parameters reported to have an effect on the N_2O production and emission were explored and discussed. Finally, the measured GHG emissions were compared to other WRRF configurations and the sources that trigger these emissions were discussed.

Table 1
Average composition and temperature of the influent of the pilot plant.

Variable	Value	Units
PO_4^{3-}	4.1 ± 1.3	g P m^{-3}
NH_4^+	39.4 ± 10.5	g N m^{-3}
NO_2^-	0.2 ± 0.4	g N m^{-3}
NO_3^-	0.2 ± 0.4	g N m^{-3}
Total COD	300 ± 128	g COD m^{-3}
Soluble COD	179 ± 62	g COD m^{-3}
Temperature	15.6 ± 4.2	°C

2. Materials and methods

2.1. Pilot plant configuration and influent

The SCEPPHAR pilot plant was located in the municipal WWTP of Manresa (Barcelona, Spain). The pilot plant was fed with the primary settler effluent of the Manresa WWTP. The average composition of the influent wastewater is shown in Table 1. The pilot plant consisted of two SBRs (R1-HET and R2-AUT), a precipitation reactor (R3-PRE) and an interchange vessel (R4-INT). The process diagram of the pilot plant is shown in Fig. 1. The R1-HET reactor was an anaerobic/anoxic/aerobic SBR (V = 2.5 m^3) designed for heterotrophic processes (EBPR, carbon removal and denitrification). The R2-AUT reactor was an aerobic SBR (V = 2.5 m^3) designed for autotrophic nitrification. R3-PRE was a precipitation reactor (V = 0.15 m^3) designed for struvite precipitation with controlled magnesium dosage. R4-INT was the interchange vessel (V = 2.5 m^3) designed for the exchange of supernatants among R1-HET, R2-AUT and R3-PRE reactors. The pilot plant operated with 70 % of volume exchange ratio of R1-HET, resulting in 1.75 m^3 of wastewater treated per cycle. The pilot plant was operated in cycles of 8- and 12-hour duration, being able to treat 5.2 and 3.5 m^3 of wastewater per day, respectively.

Each cycle of the mainstream SCEPPHAR configuration operated in the following sequence (Fig. 1): the cycle started with the filling of R1-HET, then an anaerobic phase for promoting COD fermentation, VFA uptake, PO_4^{3-} release and PHA accumulation. After an anaerobic purge to obtain a PHA-rich sludge and the settling of the reactor, the supernatant of R1-HET, rich in PO_4^{3-} and NH_4^+, was transferred to the R4-INT vessel. In R4-INT, 0.15 m^3 of the supernatant were sent to the R3-PRE reactor to precipitate struvite. The rest of the volume was transferred to the R2-AUT reactor and, once R2-AUT was filled, an aerobic phase with controlled DO took place to promote autotrophic nitritation. After the settling period, the supernatant of R2-AUT, rich in PO_4^{3-} and NO_2^- was transferred back to R1-HET. The next phase of R1-HET was an anoxic phase in which DPAO took up P while reducing NO_2^-. The last phase of R1-HET was aerobic, when PAO captured all the remaining P. After settling, the R1-HET supernatant was discharged to the effluent and the cycle started again. The detailed sequence of the cycles and the duration of each step for the 8- and 12-hour configuration are shown in Table S1 of the supplementary information (SI) section.

2.2. Pilot plant monitoring and control architecture

The pilot plant was highly equipped with online monitoring sensors and automatic control loops. R1-HET, R2-AUT and R4-INT had on-line monitoring of reactor level (Micropilot FMR20, Endress Hauser), which was key for

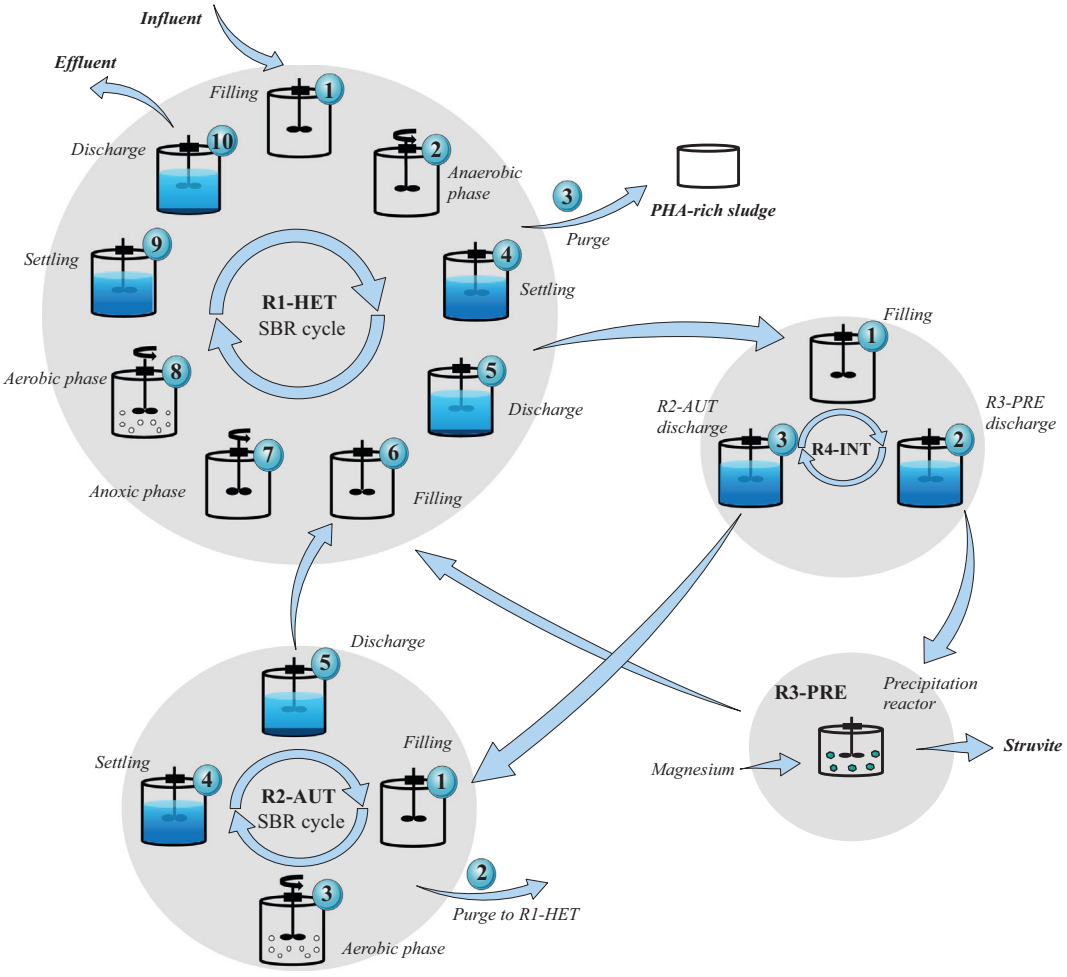

Fig. 1. SCEPPHAR pilot plant configuration and cycle operation (adapted from Larriba et al., 2020).

the automation of the interexchange steps between the reactors. The supernatants were transferred through centrifugal pumps (JP6 B-A-CVBP, Grundfos). R1-HET, R2-AUT and R3-PRE were stirred (HR4A-020/100, Milton Roy Mixing) during the reaction phases. R1-HET and R2-AUT were equipped with probes for temperature (Pt1000, Axiomatic), DO (LDO sc, Hach), pH (PC1R1N, Hach) and oxidation-reduction potential (ORP) (RC1R5N, Hach). In addition, R2-AUT was monitored with an online ion-selective electrode for ammonia (AN-ISE sc, Hach). Dosing pumps were used for sludge purge (PS2, Seko) and magnesium addition (Tekna EVO, Seko). DO in R1-HET and R2-AUT was controlled by manipulating the aeration flowrate through electric control valves (Type 3241/3374, Samson Instruments), based on the DO measurement and a proportional-integral (PI) algorithm implemented in the control system. The aeration flow to each reactor was monitored with gas rotameters (Iberfluid). The aerobic phase length in R2-AUT was controlled via the online ammonium sensor, i.e. the control system deactivated the DO PI controller and stopped the aeration when the ammonium was depleted (Larriba et al., 2020). N_2O and CH_4 gas emissions during the aerobic phases were continuously analysed via an online infra-red gas analyser (VA 3000, Horiba). The typical location of the gas measurement analyser was R2-AUT. However, in some cycles, the analyser monitored R1-HET. The dissolved N_2O in the liquid phase was monitored in R2-AUT with an on-line dissolved N_2O microsensor (N_2O-R, Unisense A/S). All the sensors and the mechanical equipment were connected to a computer (PPC-3170, Advantech) through a data acquisition system (PCI-1711U, PCLD-8710, PCLD-885 I/O, Advantech). The software AddControl developed by the research group was used for automating all the operation, monitoring and control.

2.3. Chemical analysis

Chemical analysis of the influent and effluent COD, NH_4^+, NO_2^-, NO_3^- and PO_4^{3-} concentrations was periodically performed. In addition, one cycle per week was thoroughly monitored. Soluble components were filtered with a 0.22 μm filter (Millipore). COD was analysed using Lovibond kits (COD Vario Tube Test LR and COD Vario Tube Test MR) and the MD100 spectrophotometer (Lovibond). Soluble COD (COD_S) was measured after the sample filtration while total COD (COD_T) was not filtered. NH_4^+ was measured with an ammonium analyser (AMTAXsc, Hach Lange). Phosphate was measured with an analyser based on the Vanadomolybdate yellow method (115 VAC PHOSPHAX sc, Hach-Lange). NO_2^- and NO_3^- were analysed with Ion Chromatography (DIONEX ICS-2000). Volatile suspended solids (VSS) and total suspended solids (TSS) were analysed following Standard Methods (APHA, 1995).

2.4. GHG emissions and emission factor calculations

The N_2O gas concentration (in mg m^{-3}) in the off-gas was calculated with Eq. (1):

$$C_{N-N_2O}\left[\text{mg m}^{-3}\right] = \frac{C_{N-N_2O}[\text{ppmv}] \cdot P[1\ \text{atm}] \cdot MW_{N-N_2O}\left[28\ \text{g mol}^{-1}\right]}{R\left[0.082\ \text{atm L mol}^{-1}\ \text{K}^{-1}\right] \cdot T[\text{K}]} \quad (1)$$

C_{N-N_2O} [ppmv] and T[K] are the N_2O gas concentration, provided by the Horiba analyser, and temperature. MW_{N-N_2O} is the N_2O molecular weight and R is the gas constant. The emission flowrate for N_2O was calculated with Eq. (2):

$$N_2O\ \text{emission rate}\left[\text{g d}^{-1}\right] = C_{N-N_2O}\left[\text{mg m}^{-3}\right] \cdot Q_{gas}\left[\text{m}^3\ \text{d}^{-1}\right] \cdot \left[\frac{1\text{g}}{1000\ \text{mg}}\right] \quad (2)$$

where Q_{gas} is the aeration flowrate, given by the data acquisition system of the pilot plant. Finally, the total N_2O emitted per cycle is calculated with Eq. (3):

$$N_2O\ \text{emitted}\ [\text{g}] = \Sigma_{i=1}^{n}\left(N_2O\ \text{emission rate}\left[\text{g d}^{-1}\right] \cdot \Delta t\ [\text{d}]\right)_i \quad (3)$$

where Δt is the time interval for off-gas N_2O recording (1 min) and n is the total number of data points recorded in the cycle. CH_4 emission was analogously calculated using Eq. (1) for CH_4 concentration (in ppmv), using the CH_4 molecular weight (16 g mol^{-1}).

Finally, the N_2O emission factor (N_2O-EF) of each cycle was calculated as the percentage of N_2O-N emitted during the cycle (in R2-AUT or R1-HET) of the total influent NH_4^+-N load (Eq. (4)). Similarly, The CH_4 emission factor (CH_4-EF) was calculated as the percentage of influent COD emitted as CH_4 (Eq. (5)).

$$N_2O - EF\ [\%] = \frac{N_2O - N\ \text{emitted}}{NH_4^+ - N_{infl} \cdot VOL_{infl}} \cdot 100 \quad (4)$$

$$CH_4 - EF\ [\%] = \frac{CH_4\ \text{emitted}}{COD_{infl} \cdot VOL_{infl}} \cdot 100 \quad (5)$$

where NH_4^+-N_{infl} and COD_{infl} are the ammoniacal nitrogen and COD influent concentrations, respectively, and VOL_{infl} is the influent volume (1.75 m^3). In the cycles where the emissions were measured in both R1-HET and R2-AUT, the total emission factor was calculated as the sum of the emission factor in each reactor.

3. Results

3.1. Long term operation of the pilot plant

The SCEPPHAR pilot plant was operated for two years. The operation of the plant was divided into three periods (Larriba et al., 2020):

- Period I (first three months) corresponded to the start-up of the pilot plant. During this period, the operation was adapted to achieve complete nitrification and EBPR.
- Period II (from day 0 to 225) corresponded to the operation under complete nitrification and high PAO activity. The pilot plant met the effluent legal discharge limits.
- Period III (from day 275 to 700) corresponded to the N removal via nitrite while maintaining good PAO activity and meeting the legal discharge limits. The plant operation was optimized by decreasing of the cycle length from 12 to 8 h or by implementing different aeration strategies.

The results showed in this study belong to the last 300 days of operation of period III in which the pilot plant achieved N removal via nitrite and GHG emissions were monitored in selected cycles of the pilot plant.

3.2. Process performance of the pilot plant

Fig. 2 shows the influent and effluent profiles for NH_4^+, PO_4^{3-} and COD and the effluent profiles for NO_2^- and NO_3^- of the pilot plant during the last 300 days of operation. The influent NO_2^- and NO_3^- values are shown in Table 1. NH_4^+ effluent concentration was 6.0 ± 7.3 g NH_4^+-N m^{-3}. EBPR performance was good during most of the time with an average effluent P of 0.72 ± 0.99 g PO_4^{3-}-P m^{-3}. The effluent COD average concentration was 70 ± 68 g COD m^{-3}. Effluent NO_2^-, NO_3^- and total nitrogen (TN) average concentrations were 3.2 ± 2.0 g NO_2^--N m^{-3}, 0.6 ± 0.7 g NO_3^--N m^{-3} and 11.5 ± 6.8 g N m^{-3}, respectively. Therefore, the pilot plant was meeting the required discharge legal limits most of the time, except for the ammonium (NH_4^+ < 4 g NH_4^+-N m^{-3}, P < 1 g PO_4^{3-}-P m^{-3}, COD < 125 g COD m^{-3} and TN < 10 g N m^{-3} (EEC Council, 1991)). Furthermore, good removal efficiencies were obtained for TN, P and COD: 67 ± 23 %,

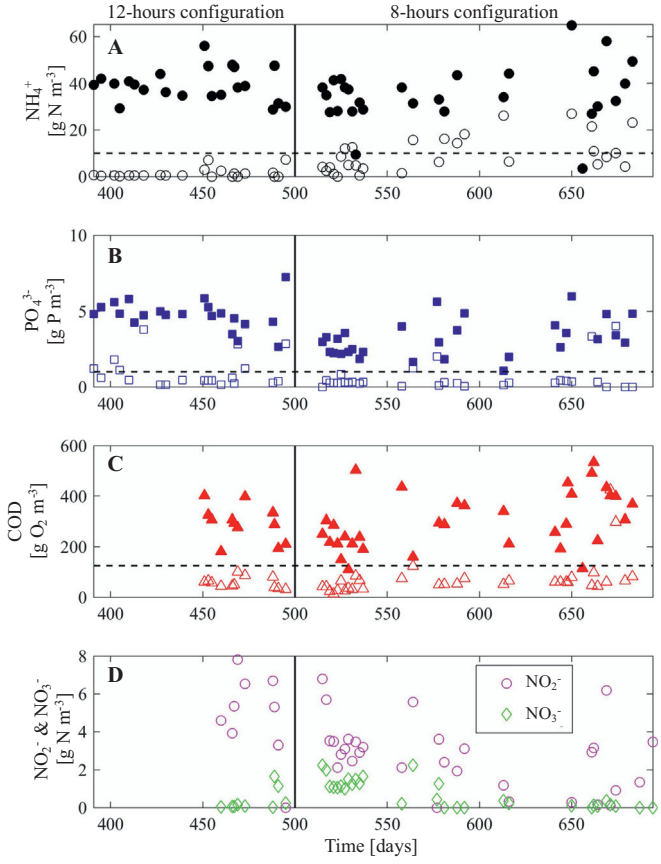

Fig. 2. SCEPPHAR pilot plant influent and effluent profiles for ammonium (A), phosphate (B) and COD (C) and effluent profiles for nitrite and nitrate (D) during the studied period. Filled symbols represent influent concentration while void symbols represent effluent concentration. Dashed line represents discharge limit for TN (A), P (B) and COD (C).

82 ± 24 % and 76 ± 18 %, respectively. The averaged solids concentration in R1-HET and R2-AUT were similar: 2.45 ± 0.28 and 2.39 ± 0.39 gVSS·m^{-3} in R1-HET and R2-AUT, respectively, and 2.80 ± 0.40 and 2.86 ± 0.54 gTSS·m^{-3} in R1-HET and R2-AUT respectively.

On day 500, the cycle was shortened to 8 h and the pilot plant removal efficiencies for TN, P and COD were maintained (Fig. 2), while the plant volumetric capacity increased by 50 %. Shortcut N-removal was achieved during the operational period III: the effluent concentration of NO_2^- was always higher than that of NO_3^- (Fig. 2D). Shortcut N-removal was successfully attained by applying two control strategies simultaneously at a DO set point (DO_{SP}) of 3 g O_2 m^{-3}. Both strategies aimed at reducing NOB activity while maintaining high AOB activity: i) the real-time control length of the aerobic phase in R2-AUT using the on-line NH_4^+ measurement and ii) operating with a selected sludge retention time (SRT) to remove NOB while retaining AOB. The first strategy is based on stopping the aeration when NH_4^+ is depleted. Then, NO_2^- should be accumulated due to the lack of oxygen and NOB growth would be limited (Guo et al., 2009; Marcelino et al., 2011). The second strategy relied in operating with a selected SRT to remove NOB faster than their growth rate (Jubany et al., 2009), Eq. (6):

$$\mu_{NOB,app} < SRT^{-1} < \mu_{AOB,app} \quad (6)$$

where $\mu_{NOB,app}$ and $\mu_{AOB,app}$ are the apparent growth rate of NOB and AOB, respectively, i.e. the apparent specific growth rate minus the apparent decay rate for each bacteria. This optimal SRT value depends on the operational conditions that affect the apparent growth rate (i.e. DO, T and pH). To implement this strategy in the plant, a stepwise increase of R2-AUT purge was applied to decrease the SRT until detecting high nitrite and low nitrate concentration at the end of the aeration phase. Both the control of the aeration phase length and the fixed SRT led to a gradually decrease of the NOB population and a subsequent increase on NO_2^- accumulation at the end of aerobic phases (Larriba et al., 2020).

Fig. 3 shows an example of the SCEPPHAR cycle operation (day 410), when the pilot plant was operated under a 12-hour cycle configuration. Fig. 4 shows all the monitored variables of the pilot plant for the same cycle. The influent composition for this cycle was 5.8 g PO_4^{3-}-P m^{-3} and 41.0 g NH_4^+-N m^{-3}. The cycle started with the feeding of R1-HET (step 1 of R1-HET in Fig. 1 and Table S1 of SI). The first measurement just after the feeding ended (time = 0.63 h, Fig. 4A) was 14.8 g PO_4^{3-}-P, showing that during the feeding some P was released by PAO. During the second step of R1-HET, the anaerobic phase, the PO_4^{3-} concentration increased up to 31.8 g P m^{-3} (Fig. 3A) due to the P-release linked to VFA consumption by PAO. The ORP probe (Fig. 4D) shows that anaerobic conditions were reached (ORP value below zero) after the feeding of the reactor was completed. The ORP probe signal stabilized at 3 h of the cycle while complete anaerobic conditions were maintained. When the anaerobic phase ended (at time = 6 h), part of the biomass was purged (step 3) and the supernatant of the reactor was settled (step 4). Then, the supernatant accounting for 70 % of R1-HET volume was transferred to the interchange reactor R4-INT (step 5). The following step of R1-HET (step 6) was the filling of the reactor with the supernatants from R2-AUT (from the previous cycle) and R3-PRE. Then, the anoxic phase started (step 7). At the beginning of the anoxic phase, the PO_4^{3-} concentration (Fig. 3A) decreased to 24.1 g P m^{-3} (compared to that the end of the aerobic phase of R2-AUT) due to: i) struvite precipitation decreased the P concentration of the supernatant of R3-PRE returned to R1-HET, ii) slightly decrease on the P concentration due to P-uptake in R2-AUT (Fig. 3B) and iii) decrease on P concentration during the filling process of R1-HET due to anoxic conditions. The NH_4^+ concentration considerably decreased due to the dilution of R1-HET, since the NH_4^+ concentration in the supernatant from R2-AUT returned to R1-HET was negligible. During the anoxic phase, the remaining NO_2^- was used by DPAO as the electron acceptor. In the presented cycle, NO_2^- concentration at the beginning of the anoxic phase was already negligible, meaning that all NO_2^- was denitrified during the anoxic filling period of R1-HET. Therefore, the observed P-uptake during the anoxic phase was low (2.0 g PO_4^{3-}-P m^{-3}). Soluble COD and NH_4^+ remained constant during the anoxic phase. The next step of R1-HET reactor was the aerobic phase (step 8). This cycle showed successful P-uptake, obtaining 0.4 g PO_4^{3-}-P m^{-3} at the end of the aerobic phase (DO_{SP} = 3 g O_2 m^{-3}). NH_4^+ was oxidised to 0.5 g N m^{-3} and NO_3^- was not observed in R1-HET. NO_2^- concentration at the end of aerobic phase was 7.9 g NO_2^--N m^{-3}(Fig. 3A). ORP probe signal sharply increased with the presence of oxygen as electron acceptor (Fig. 4D). When the aerobic phase ended, aeration and stirring were turned off, supernatant was settled (step 9) and discharged to the effluent (step 10), fully accomplishing discharge limits.

In R2-AUT, the cycle started with the reactor filling with the supernatant of R1-HET (step 1 of R2-AUT in Fig. 1). Once the reactor was filled, the second step was the purge of the reactor (step 2). The aerobic phase (step 3) started after an idle phase at 0.63 h of the cycle. Temperature was constant during the aerobic phase (Fig. 4C), with an average value of 24.2 °C. At a DO_{SP} of 3 g O_2 m^{-3}, all the NH_4^+ was oxidised to NO_2^- rather than to NO_3^-, showing that there was a reduced NOB activity during this cycle. The NH_4^+ online sensor showed a constant AOR during the aeration of the reactor, with a value of 8.5 g NH_4^+-N m^{-3} h^{-1} (R^2 = 0.99). The DO control system opened the aeration valve at the beginning of the aerobic phase (Fig. 4F) to rapidly achieve the desired DO_{SP} and gradually closed it considering the decrease on the NH_4^+ concentration. In addition, the aerobic length control turned off the aeration after 2.4 h of aerobic phase (maximum duration 3 h), when the ion-selective NH_4^+ probe signal was 3 g NH_4^+-N m^{-3}. The sharp drop in the N_2O profile (Fig. 3C) was a consequence of the stop of aeration, which eliminated N_2O stripping and thus its emissions. pH slightly decreased due to nitritation (Fig. 4B). The redox

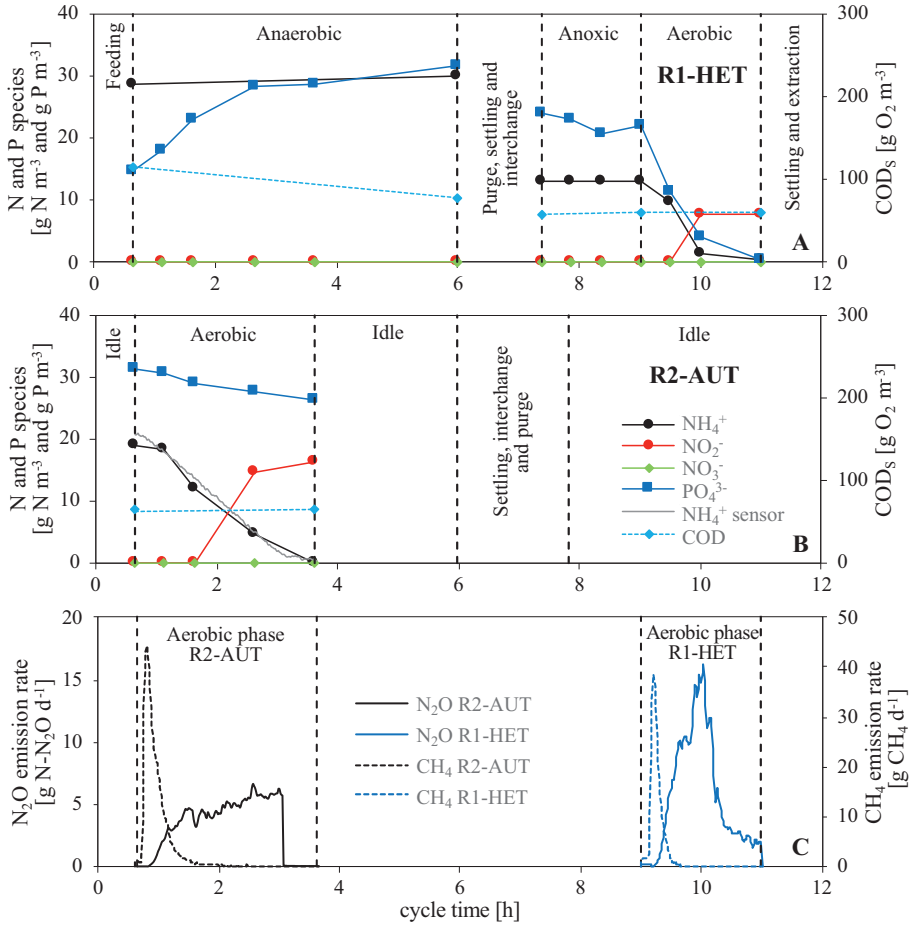

Fig. 3. Example of SCEPPHAR cycle operation (A and B) and GHG profiles (C) obtained for R1-HET and R2-AUT with a cycle length configuration of 12 h (cycle belonging to day 410 of operation).

potential increased with the DO and the NO_2^- accumulation as electron acceptors (Fig. 4D). Fig. 3B reveals some P-removal in R2-AUT (4.9 g PO_4^{3-}-P m^{-3}), probably due to interchange of some biomass between reactors and the long idle period of R2-AUT, acting as a post anaerobic zone (Larriba et al., 2020; Wang et al., 2012). The rest of the R2-AUT steps were the settling and discharge to R1-HET (steps 4 and 5, respectively, Fig. 1).

Finally, the R3-PRE reactor received 0.15 m^3 of supernatant from R4-INT with high content of PO_4^{3-} and NH_4^+. P precipitation took place after the air sparging to increase pH and the addition of magnesium solution (19 g Mg^{2+} m^{-3} as $MgCl_2$). Typically, P concentration decreased around 70 % (Larriba et al., 2020) in R3-PRE. Finally, the supernatant of R3-PRE, with low content in PO_4^{3-} and NH_4^+ was sent to R1-HET (Fig. 1).

An example of a fully monitored SCEPPHAR cycle for an 8 h cycle configuration on day 557 is shown in Figs. S1 and S2 of SI section. This cycle was operated at the same DO_{SP} of 3 g O_2 m^{-3} (Fig. S2E of SI). The profiles obtained in Fig. S1A of SI section show that the pilot plant was able to obtain a high effluent quality with reduced anaerobic and anoxic phases length in R1-HET and the observations were similar to those obtained on day 410 (Figs. 3 and 4). However, although NH_4^+ concentration obtained at the end of aerobic phase of R2-AUT was below discharge limits (2.9 g NH_4^+-N m^{-3}), the AOR achieved (7.1 g NH_4^+-N m^{-3} d^{-1}) was lower than that on day 410 and the aerobic phase was extended to the maximum length value allowed (3 h). This fact is probably due to VSS concentration being 14 % lower in the 8-hour cycle period than in the 12-hour cycle period.

3.3. Overall GHG emissions of the pilot plant

During part of period III, N_2O and CH_4 emissions were monitored during the aerobic phases of the reactors. Table 2 shows the average N_2O and CH_4 emitted per cycle and the corresponding emission factors (Eqs. (4) and (5)) obtained for the configurations of 8 (n = 13) and 12 h (n = 21). In addition, Figs. 3C and S1C show the N_2O and CH_4 emission profiles for typical SCEPPHAR cycles of 12 and 8 h length.

The GHG emissions were monitored for a total of 43 cycles with 12-hour configuration and 18 cycles for the 8-hour configuration. The cycles in Table 2 were those with the usual operation at a DO_{SP} of 3 g O_2 m^{-3}. Overall, the N_2O emissions in R2-AUT were higher than those in R1-HET because most of the NH_4^+ was nitrified in R2-AUT (Table 2). The N_2O emissions (around 0.7 g N_2O-N per cycle) and N_2O-EF (around 1.0 %) were low compared to similar SBR systems (Massara et al., 2017) for both cycle length configurations. The SCEPPHAR configuration was capable to maintain low emissions despite NO_2^- being accumulated in the reactors. The measured N_2O emissions and N_2O-EF were approximately the same operating at 12 and 8 h since both configurations had the same aerobic phase length and similar average temperatures (21.8 ± 2.6 °C for 8 h and 22.3 ± 0.8 °C for 12-hour configuration). Figs. 3C and S1C show how N_2O emissions began when NH_4^+ was being nitrified and the emissions decreased to zero when both aeration and reactor mixing stopped. N_2O emissions from R1-HET were higher than those from R2-AUT, which can be attributed to the higher aeration flowrate required in R1-HET to achieve the same DO_{SP}, increasing N_2O stripping. In any case, the factors affecting these N_2O emissions are further examined in Section 3.4, where the different DO control strategies implemented are reported.

Regarding CH_4 emissions, lower variability on the emissions were measured compared to N_2O emissions, since the aeration strategy has no effect on the CH_4 production. Table 2 shows that CH_4 emissions measured during the operation of the pilot plant were low, with <1.0 g CH_4 emitted per cycle

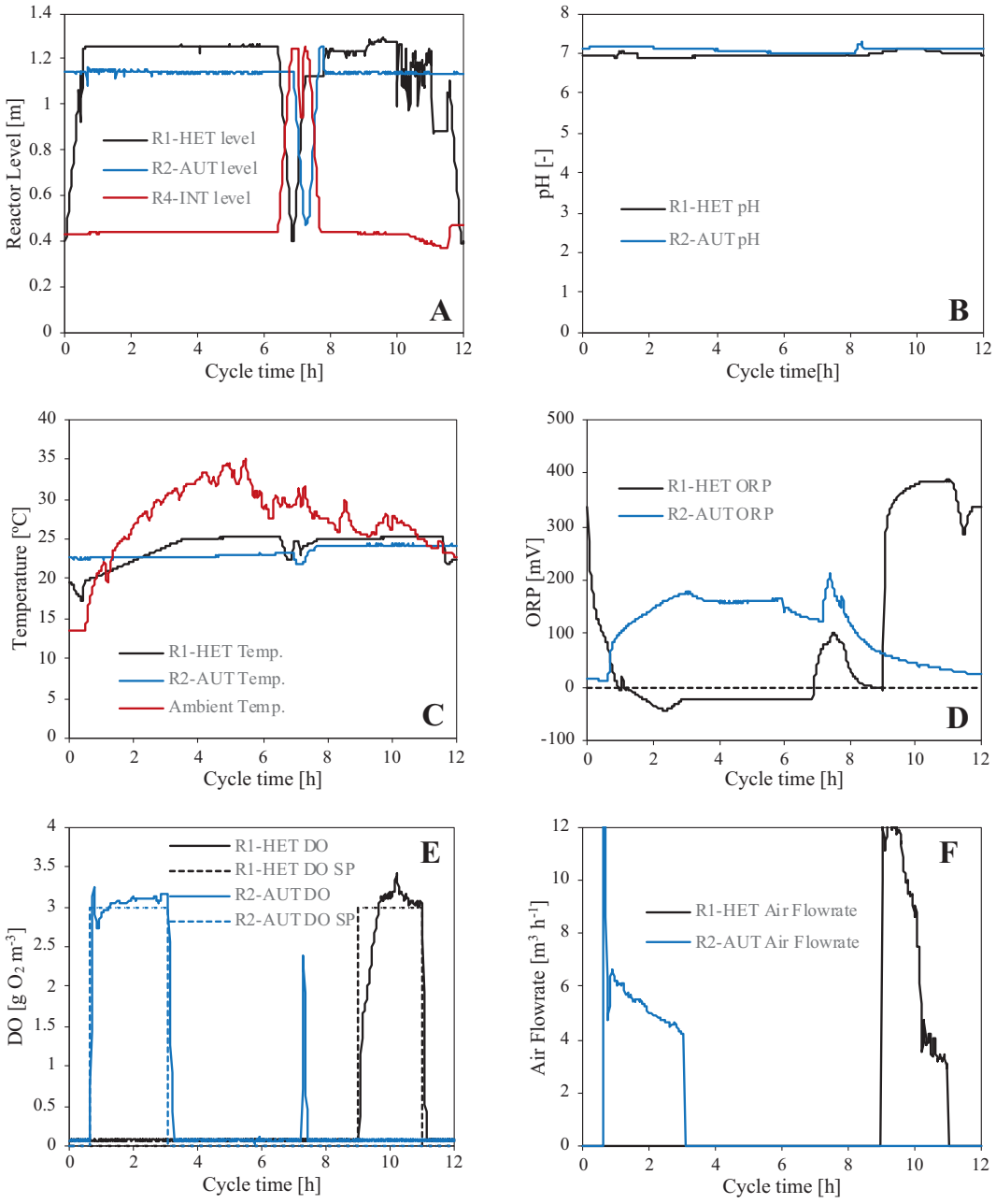

Fig. 4. Online monitored variables for an example of SCEPPHAR cycle operation with a cycle length configuration of 12 h (cycle belonging to day 410 of operation).

and a CH_4-EF lower than 0.20 %. CH_4 emissions were clearly higher in R2-AUT than in R1-HET and the emission rates showed a peak shape (Figs. 3C and S1C). On one hand, the CH_4 emission rate had an initial peak since CH_4 was not produced during aerobic conditions but the dissolved CH_4 was only stripped from the liquid phase to the gas phase. On the other hand, CH_4 emissions were higher in R2-AUT compared to R1-HET due to the sequence of wastewater treatment in the SCEPPHAR configuration (Fig. 1): air is sparged to the wastewater for the first time in the aerobic phase of R2-AUT. Therefore, the emitted CH_4 in R2-AUT was probably introduced dissolved in the influent wastewater, while a slight amount might be produced

Table 2
Average N_2O and CH_4 emissions and emissions factors measured for the cycle length configurations of 12 (n = 21) and 8 (n = 13) hours. Standard deviation is presented.

Cycle length →	12 h			8 h		
Reactor →	R1-HET	R2-AUT	Total	R1-HET	R2-AUT	Total
N_2O [g N_2O-N]	0.19 ± 0.18	0.44 ± 0.15	0.64 ± 0.24	0.27 ± 0.23	0.42 ± 0.37	0.69 ± 0.43
N_2O-EF [%]	0.28 ± 0.26	0.64 ± 0.22	0.93 ± 0.34	0.39 ± 0.33	0.61 ± 0.53	1.00 ± 0.62
CH_4 [g CH_4]	0.25 ± 0.23	0.57 ± 0.19	0.82 ± 0.30	0.06 ± 0.03	0.36 ± 0.34	0.42 ± 0.34
CH_4-EF [%]	0.05 ± 0.04	0.11 ± 0.04	0.16 ± 0.06	0.01 ± 0.01	0.07 ± 0.06	0.08 ± 0.06

during the anaerobic phase in R1-HET. Therefore, the existing lower CH_4 emissions in R1-HET during the aerobic phase were due to the 30 % of reactor volume that was not interchanged. Table 2 also reveals that the averaged CH_4 emissions from the 12-hour configuration were 50 % higher than those measured through the 8-hour configuration since, in the first case, the anaerobic phase was 55 % longer. That supports the hypothesis that part of the CH_4 emitted in R2-AUT could be produced during the anaerobic phase of R1-HET.

3.4. Effect of the aeration strategy on N_2O emissions

This section shows the effect of the different aeration strategies on N_2O emissions. During this period, some changes were made on the pilot plant cycle configuration: i) the cycle length was extended to 12 h, ii) the aerobic phase length of the R2-AUT was incremented to 7.4 h and iii) the aerobic phase length control through the NH_4^+ ion selective probe was deactivated. These changes were made to allow a more detailed study of N_2O emissions during nitrification in R2-AUT. In addition, a liquid N_2O probe was installed in R2-AUT to monitor the dissolved N_2O concentration in order to better understand the effect of the different aeration strategies on both N_2O production and emission.

The aeration strategies implemented are divided into: i) Different DO_{SP}, ii) intermittent aeration and iii) steps on the DO_{SP}. This section reports only the results related to R2-AUT reactor, where dissolved N_2O and N_2O gas emission were measured. During these pilot plant experiments, the operation of R1-HET was the same as showed in Table S1 of SI section and the reactor was operated with a constant DO_{SP} of 3 g O_2 m^{-3} in the aerobic phase.

3.4.1. Different DO_{SP}

The first set of experiments was conducted to assess the effect of different DO_{SP} on the overall N_2O production and emission. The cycles were operated at three different DO_{SP}: 1, 2 and 3 g O_2 m^{-3}. Table 3 shows the obtained average N_2O emissions and N_2O-EF in R2-AUT. Fig. 5 shows the profiles of DO, air flowrate, N_2O emission, soluble N_2O concentration and NH_4^+ concentration for three cycles at a DO_{SP} of 1, 2 and 3 g O_2 m^{-3}.

Fig. 5A shows that the DO in R2-AUT could be controlled properly at different DO_{SP} and Fig. 5E shows that full NH_4^+ oxidation was achieved regardless of the DO_{SP}. The oscillations in DO concentration and air flowrate measured at the end of the aerobic phase (Fig. 5A and B) were due to the low linearity of the valve in the low range of actuation (valve opening below 25 %), which makes it difficult for the PI controller to maintain a stable DO concentration. The AOR was very similar among the cycles: 3.48, 3.72 and 3.57 g N m^{-3} h^{-1} ($R^2 > 0.98$) for DO_{SP} of 1, 2 and 3 g O_2 m^{-3}, respectively, showing that the AOR was not dependent on DO in the range of values tested. Regarding N_2O emissions, a different trend in N_2O emission was observed in each cycle when compared to the examples of pilot plant cycles in Figs. 3 and S1. Fig. 5C shows that a N_2O emission peak was obtained for the three cycles at the beginning of the aerobic phase of R2-AUT regardless of the DO_{SP}. Then, it decreased rapidly to lower constant emission rate until NH_4^+ depletion. This initial emission peak accounts from 20 % up to 60 % of the total N_2O emission measured per cycle for the cycles operated at 2 and 3 g O_2 m^{-3} (Fig. 5) and could be correlated to the dissolved N_2O: a similar peak was detected in the three cycles on the dissolved N_2O profile (Fig. 5D). Moreover, the higher the dissolved N_2O value, the higher the N_2O emission peak. The independency from the DO_{SP} on the peak emission rate is due to the aeration control system fully opened the air distribution valve at the beginning of the aerobic phase for the three DO_{SP} (Fig. 5B). Both gas and liquid N_2O measurements (Fig. 5C and D) show that N_2O was continuously produced during the pilot plant cycle, since dissolved N_2O was being accumulated and N_2O was continuously emitted. A strong correlation between the stripping of dissolved N_2O and the DO_{SP} was found; dissolved N_2O increased when operating at lower DO_{SP} (i.e. with lower aeration flowrate) and the N_2O emissions decreased due to a reduction on the mass transfer coefficient. However, the impact of the stripping effect was not relevant in these cycles since most of the N_2O emission was found at the beginning of the aerobic phase during the emission peak, where the air flowrate was the same for the three DO_{SP}. Finally, Fig. 5D shows that the dissolved N_2O concentration decreased due to stripping to the gas phase when ammonium was depleted and NO_2^- was accumulated for the cycles operated at 2 and 3 g O_2 m^{-3}. Table 3 shows that no correlation was found between the operating DO and the total N_2O emissions due to the high variability observed on the N_2O emissions even at the same DO_{SP}: the average N_2O emissions from the cycles operated at DO of 2 g O_2 m^{-3} were higher than those obtained when operating at a DO of 1 g O_2 m^{-3} and of 3 g O_2 m^{-3}. In addition, the variability found in N_2O emissions for the cycles operating at the same DO_{SP} was similar to that calculated for the cycles operated at different DO_{SP}. Therefore, in our case, the DO concentration seems to have no effect on the N_2O emissions of the pilot plant, probably because the same AOR was achieved at different DO concentrations.

Table 3
Average N_2O emissions and N_2O-EF measured in R2-AUT per cycle for different DO set-points. n represents the number of cycles operated at each DO set-point. Standard deviation is presented.

DO set-point [g O_2 m^{-3}]	N_2O emission [g N_2O-N]	N_2O-EF [%]
1 (n = 7)	0.34 ± 0.27	0.50 ± 0.39
2 (n = 6)	0.53 ± 0.30	0.76 ± 0.43
3 (n = 34)	0.43 ± 0.48	0.62 ± 0.70

3.4.2. Intermittent aeration

The second set of experiments was conducted to assess the effect of intermittent aeration on the overall N_2O production and emission. The intermittent aeration was implemented as an on/off controller where the reactor was aerated at a constant air flowrate and aeration was stopped when the DO measurement increased above 2 g O_2 m^{-3} and was turned on again for DO below 1 g O_2 m^{-3}. This on/off control was maintained throughout the aerobic phase of R2-AUT. The pilot plant was operated with on/off aeration control under two different air flowrates: 12.5 and 5.0 m^3 h^{-1} (100 and 40 % of the maximum air flowrate, respectively). Fig. 6 shows the profiles of DO, air flowrate, N_2O emission, dissolved N_2O concentration and NH_4^+ concentration for two typical cycles with on/off control.

Fig. 6A shows the variability of the DO concentration for both implemented air flowrates through intermittent aeration. The DO ranged between 0.6 and 2.8 g O_2 m^{-3} for the high air flowrate and between 0.6 and 2.0 g O_2 m^{-3} when the pilot plant was operated at 40 % of the maximum air flowrate and NH_4^+ was not depleted. DO values outside the range 1–2 g O_2 m^{-3} were due to the dynamics of the DO sensor and the control valve, even though the on/off controller was sending the command to close the aeration when the measured DO was 2 g O_2 m^{-3} and was sending the command to open it when DO was 1 g O_2 m^{-3}. The DO concentration at high airflow rate achieved 2 g O_2 m^{-3} at 10 min of aerobic phase, while it lasted 2 h in the experiment operated with the low air flowrate of 5 m^3 h^{-1} (Fig. 6B). The duration of the on phases decreased in time for both air flowrates meanwhile the oxygen uptake rate decreased due to lower NH_4^+ concentration. The same NH_4^+ concentration was measured for both cycles at the beginning of the aerobic phase and both cycles achieved full ammonia oxidation to nitrite. The same AOR was achieved for both cycles (2.70 g N m^{-3} h^{-1}, R^2 = 0.99), showing that the AOR was not significantly different although the average DO levels were slightly different (1.4 vs 1.8 g O_2 m^{-3} for low and high flowrate). The same fact was observed in results of Section 3.4.1. The NH_4^+ concentration decreased linearly over the time, without any strong variation in the AOR due to the on/off aeration cycles.

Regarding the N_2O results, a peak of dissolved N_2O was measured in the reactor at the beginning of the aerobic phase for both cycles (Fig. 6D), as in the cycles operated at different DO_{SP} (Fig. 5, Section 3.4.1). This peak of dissolved N_2O caused a N_2O emission peak at the beginning of the aerobic phase (Fig. 6C), however, the emission decreased to negligible levels in the off phases since stripping was suppressed (high flowrate scenario).

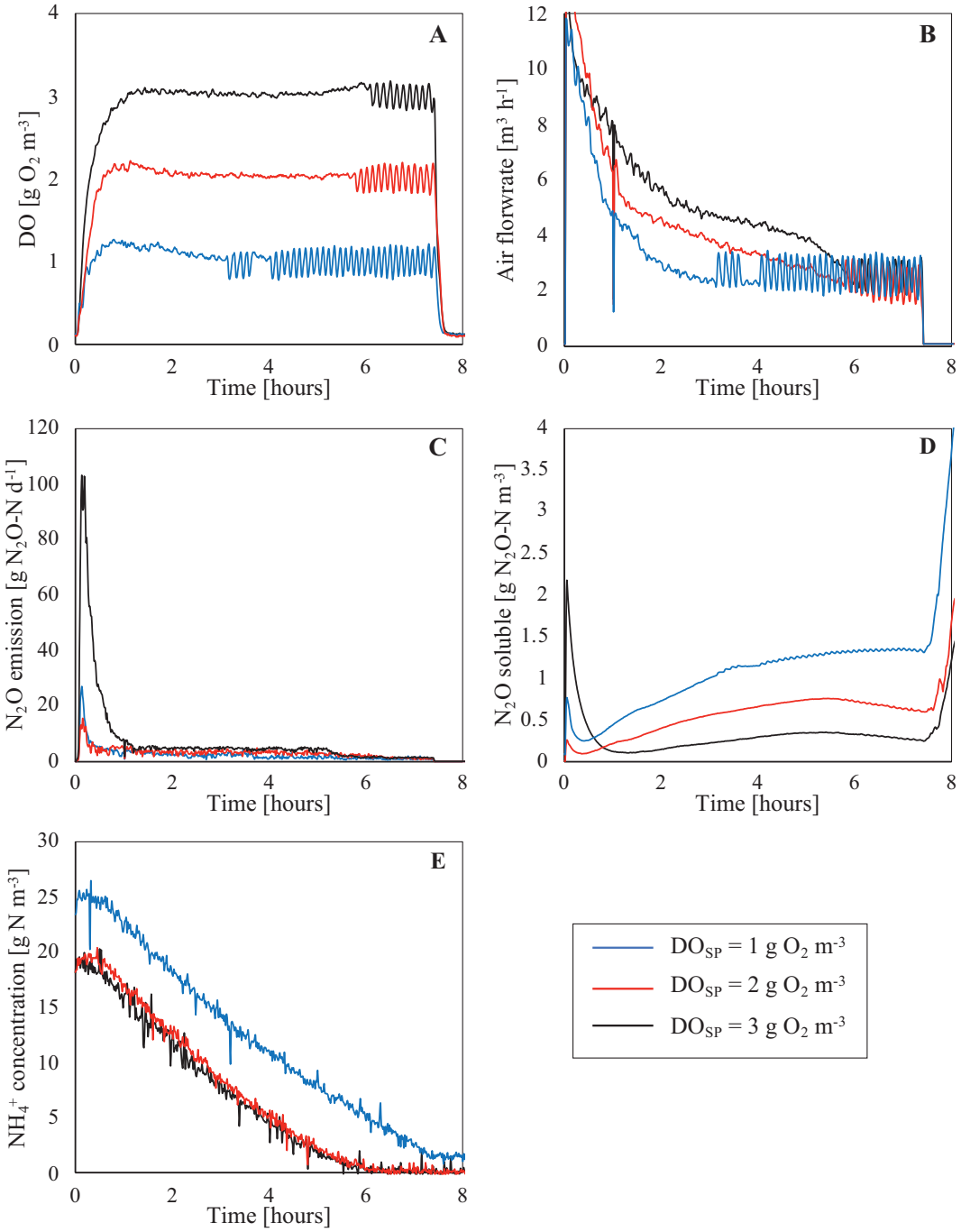

Fig. 5. Selected monitored variables for three examples of SCEPPHAR operation with extended aeration phase length in R2-AUT using different DO set-points. (A) DO, (B) air flowrate, (C) N_2O emission rate, (D) soluble N_2O concentration and (E) ammonium online concentration.

This behaviour was not observed in the cycle operated at a low air flowrate because the emission peak finished before the first off phase. The dissolved N_2O measurements shows that there was no accumulation of N_2O in the liquid phase during all the aerobic phase for both cycles. The net N_2O production seemed null since: i) the dissolved N_2O concentration decreased constantly once the initial peak was stripped to the gas phase, and ii) the N_2O liquid concentration remained constant during the initial peak during the off phase of the cycle operated with the high air flowrate (zoom of Fig. 6D). A possible explanation is that simultaneous nitrification-denitrification was taking place and N_2O was simultaneously produced and consumed. The R2-AUT N_2O-EF measured for the cycles operated at 12.5 and 5.0 $m^{-3}\ h^{-1}$ were 0.40 and 0.48 %, respectively (Fig. 6). However, no correlation was found between the air flowrate and the emitted N_2O. The averaged R2-AUT N_2O-EF of all the cycles operated with intermittent aeration strategy (21 cycles) was 0.40 ± 0.21 %.

3.4.3. Steps on the DO_{SP}

Finally, the last set of experiments was carried out to assess the effect of varying the DO_{SP} during the same aerobic phase of R2-AUT on the N_2O stripping and emissions. Two experiments were conducted: in the first one, the DO_{SP} was increased every 2 h in a stepwise manner, testing values of 1, 2 and 3 g $O_2\ m^{-3}$. In the second experiment, the same strategy was applied but with values of 3, 2 and 1 g $O_2\ m^{-3}$. The third step of both experiments lasted until the end of the aerobic phase (3.4 h). Fig. 7 shows the profiles of DO, air flowrate, N_2O emission, dissolved N_2O concentration and NH_4^+ for both experiments.

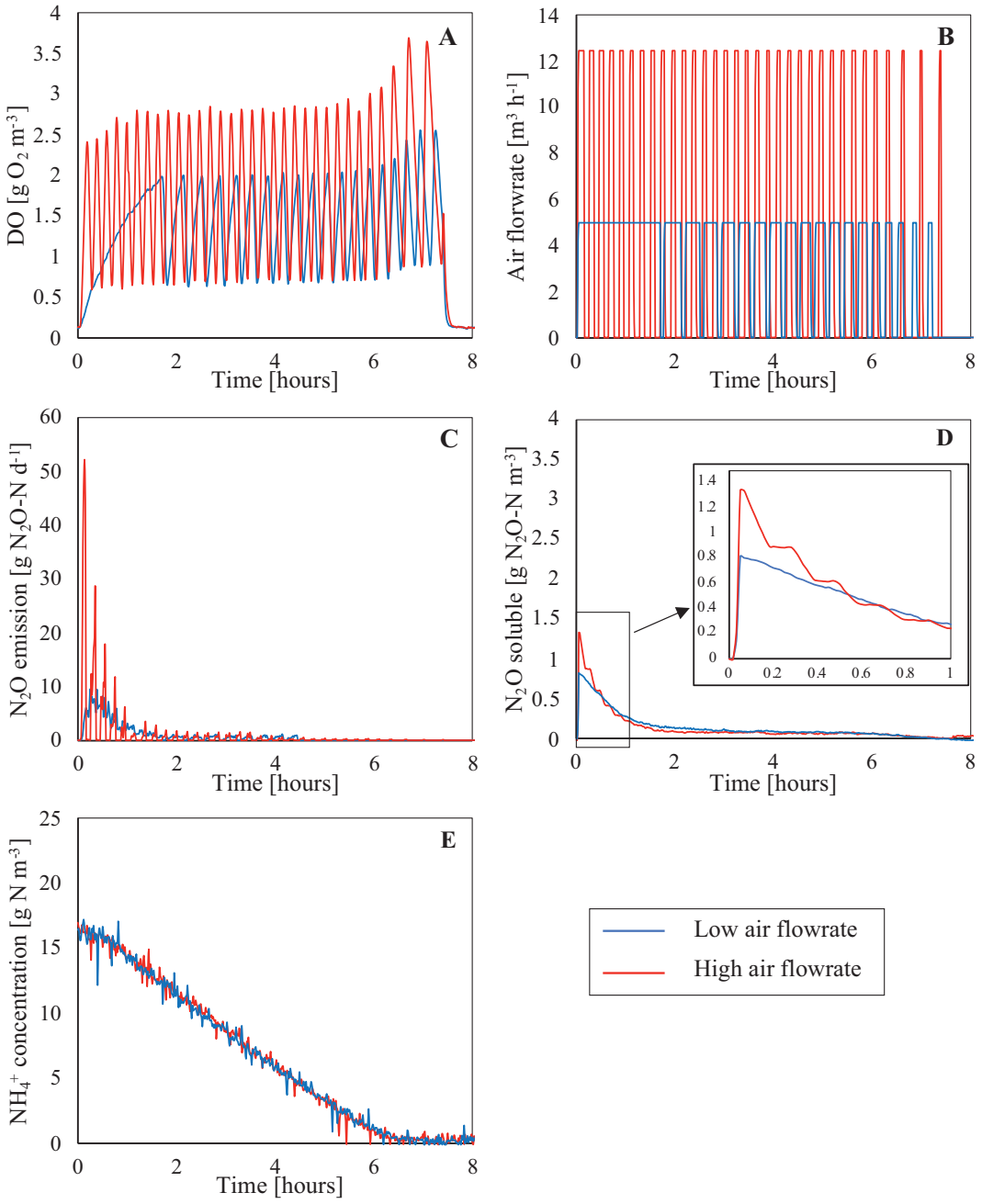

Fig. 6. Selected monitored variables for two examples of SCEPPHAR operation with extended aeration phase length in R2-AUT and using on/off aeration control at 5.0 and 12.5 $m^3\ h^{-1}$ of air flowrate. (A) DO, (B) air flowrate, (C) N_2O emission rate, (D) soluble N_2O concentration and (E) ammonium online concentration.

Fig. 7 shows that the DO PI control loop reacted fast to setpoint changes, modifying the aeration to reach effectively the new setpoint. On the first experiment, the aeration control system opened the valve up to 90 % for short periods in order to reach the increased setpoints. On the second experiment, the aeration control system closed the air control valve down to 10 % (and even fully closed) after decreasing the setpoint. Similar NH_4^+ concentrations were measured for both experiments at the beginning of the aerobic phase. The AOR of the increasing DO experiment remained constant among the DO steps (3.02 g NH_4^+-N $m^{-3}\ h^{-1}$, $R^2 = 0.98$) but the AOR of the decreasing experiment decreased from 3.9 ($R^2 = 0.80$) to 3.3 ($R^2 = 0.90$), and 2.3 g NH_4^+-N $m^{-3}\ h^{-1}$ ($R^2 = 0.83$) in parallel with the new DO_{SP} of 3, 2 and 1 g $O_2\ m^{-3}$, respectively (Fig. 7E). Interestingly, neither an initial peak of soluble N_2O nor N_2O emission was measured in any of the DO step experiment, in contrast with other experiments. Both the emission and dissolved N_2O profiles seemed to have a strong dependency on the air flowrate applied to R2-AUT. In fact, N_2O emissions depend on the air flowrate and the actual liquid N_2O concentration, while the liquid N_2O concentration depends on both the air flowrate (i.e. gas-liquid N_2O transfer because of stripping) and the DO concentration (i.e. different biological N_2O production pathways). On the one hand, the sudden opening of the air valve linked to a DO_{SP} increase caused a sudden increase on the N_2O emissions, which decreased after the DO reached the desired setpoint. These emissions led to a decrease in the soluble N_2O concentration. On the other hand, in the second experiment, the N_2O emissions decreased and the dissolved N_2O concentration increased every time the DO_{SP} was decreased as the air control valve was closing. Finally, N_2O was continuously produced in both experiments since the accumulation

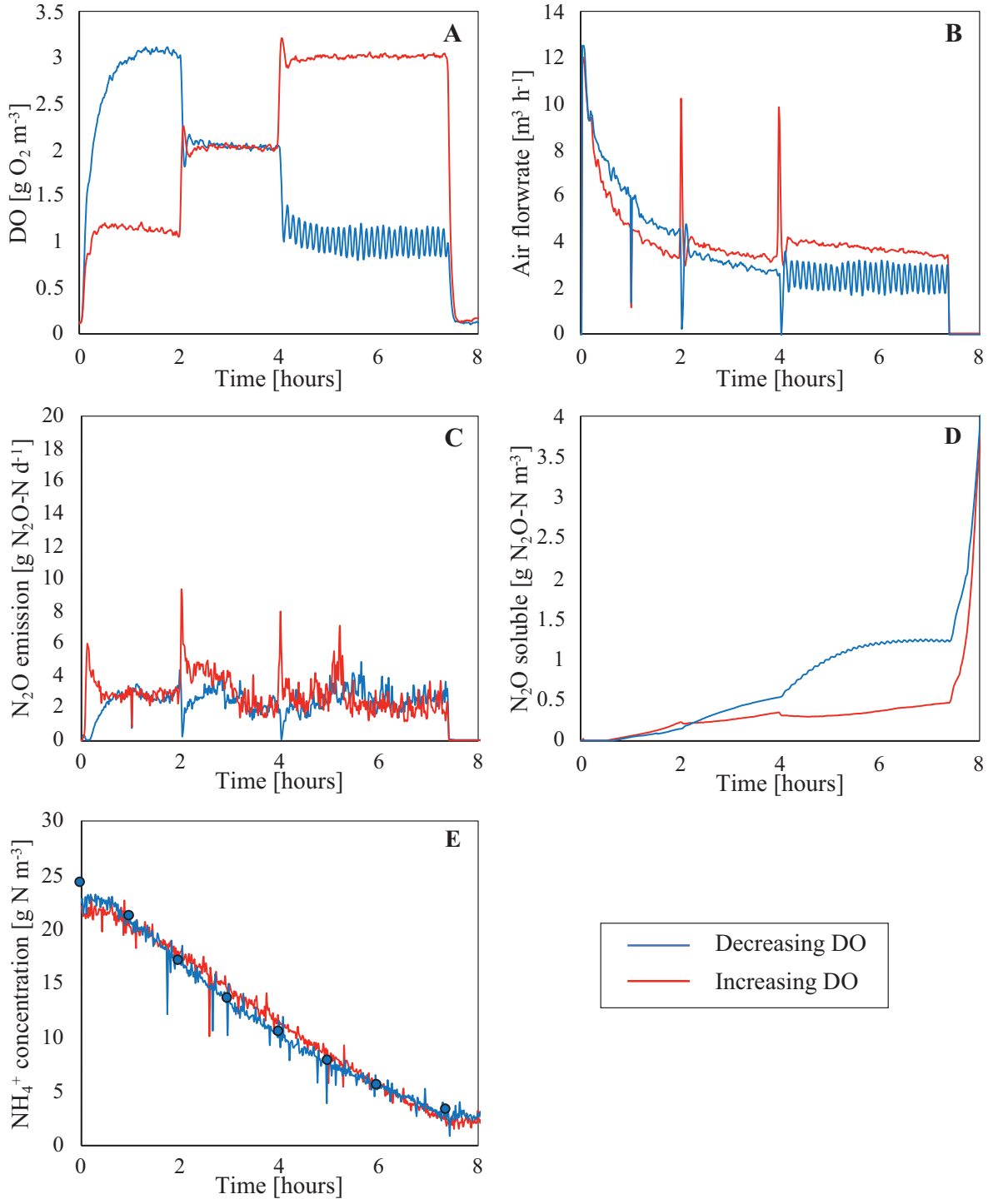

Fig. 7. Selected monitored variables for two examples of SCEPPHAR operation with extended aeration phase length in R2-AUT and different DO setpoints for the PI controller during the cycle. (A) DO, (B) air flowrate, (C) N_2O emission rate, (D) soluble N_2O concentration and (E) ammonium online concentration.

of dissolved N_2O increased in both experiments and a constant N_2O emission was measured. The accumulation of dissolved N_2O seemed to be correlated with the air flowrate, since the soluble N_2O accumulation increased in every DO_{SP} change in the second experiment: decreasing the air flowrate caused a decrease of N_2O stripping. The N_2O-EF measured in these tests was higher (1.3 % when DO was increased and 1.1 % when DO was decreased) than that achieved through intermittent aeration, because even though no initial N_2O emission peak was measured, N_2O was continuously produced during the cycles.

4. Discussion

4.1. Comparison of GHG emissions with other WRRFs

Several monitoring campaigns to quantify N_2O emissions have been conducted at different full-scale WWTPs. The main objective of the monitoring campaigns was to quantify the N_2O emissions and later to determine the factors affecting these emissions (Ahn et al., 2010; Daelman et al., 2013; Kampschreur et al., 2009; Law et al., 2012; Massara et al., 2017). These

studies have shown huge variations in the N_2O emissions in WWTPs even under similar conditions, demonstrating that it was very difficult to find a clear trend. Recent long term monitoring campaigns have been able to capture N_2O seasonal emission dynamics (Daelman et al., 2015; Gruber et al., 2020; Kosonen et al., 2016) showing significant seasonal variability with an N_2O emission factor range between 0 and 3 % of the influent N load for most of the municipal full-scale WWTPs, The variation on the N_2O-EF has been attributed to the different configurations and operational conditions in each WWTP, as well as to the inherent dynamic conditions of the plants, but probably some unknown factors are still to be discovered. Therefore, it was difficult to assess the real causes of the high N_2O-EF variations and, thus, it was difficult to design and implement novel mitigation strategies for the plant.

This study reported the long-term operation and monitoring of the mainstream SCEPPHAR configuration in a pilot scale treating real municipal wastewater. The fact that the pilot plant operated within shortcut N-removal was a priori unattractive in terms of N_2O emissions, since the accumulation of NO_2^- is a major cause of N_2O emissions. However, the average N_2O-EF calculated during the long-term operation of the whole pilot plant was 0.97 ± 0.70 %, which is in the same range for most of municipal WWTPs. This shows the capability of the mainstream SCEPPHAR configuration to obtain a high effluent quality index while reducing aeration costs and COD requirements without increasing N_2O emissions with respect to conventional nitrification/denitrification. The most likely reason for this low N_2O-EF value is the fact that this system was able to avoid nitratation while operating at a high DO_{SP}, thanks to the use of the aeration phase control. The combination of high DO (mitigates N_2O production) and relatively low airflow rate (mitigates N_2O emissions) was beneficial.

Regarding CH_4 emissions, the range in municipal WWTPs is typically from 0.02 to 1.13 % of the inlet COD (Daelman et al., 2013; Ribera-Guardia et al., 2019; Rodriguez-Caballero et al., 2014). The average CH_4-EF measured in this study was 0.12 ± 0.08 % which is in the lower band of the values reported. Regarding the possible production of CH_4 during the anaerobic phase of R1-HET, textbook knowledge states that methanogenesis is favoured under mesophilic conditions (T around 37 °C), strict anaerobic conditions and non-limiting acetate concentration for acetoclastic methanogens. However, it was experimentally observed that CH_4 emissions decreased by 50 % when the anaerobic phase was shortened by 55 % suggesting that a non-negligible amount of the emitted CH_4 was produced during the anaerobic phase of the R1-HET cycle. The presence of methanogens in the planktonic biomass can probably be discarded, as this sludge undergoes aerobic conditions during part of the cycle, while methanogens are strictly anaerobic. However, the presence of some methanogens in the possible biofilm of the reactor walls and in the sediments that can be accumulated at the bottom of the reactor could explain this slight methane production. The CH_4 present at the end of the anaerobic phase is stripped/emitted during the posterior aerobic phase.

4.2. Factors affecting N_2O emissions

N_2O emissions occurred throughout all the long-term operation. High variability was detected not only due to the applied operational changes but also when operating the plant under the same operational conditions. The DO_{SP} in R2-AUT did not seem to have any effect on the overall N_2O emissions, since no correlation was found between the DO concentration in R2-AUT and the measured emissions during the operation at different DO_{SP} between 1 and 3 g O_2 m^{-3} (Fig. 5 and Table 3). This fact is in disagreement with previous experimental reports where a decrease in the DO level led to an increase of the N_2O emissions (Massara et al., 2017; Peng et al., 2015). A possible explanation to this is that the lowest DO_{SP} implemented was 1 g O_2 m^{-3}, which probably was not low enough to trigger the increase of N_2O production. In this sense, Peng et al. (2015) measured the highest N_2O emissions among different NO_2^- accumulations at 0.35 and 0.85 g O_2 m^{-3} through a range of applied DOs from 0.35 to 3.5 g O_2 m^{-3}.

Another interesting observation was that the AOR was neither dependent on the DO concentration, as the same apparent AOR was found during the implementation of different DO_{SP}s during nitrification in R2-AUT. However, the AOR changed during the long-term operation of the pilot plant under different conditions, showing a high variability from 8.5 to 2.3 g N m^{-3} h^{-1}. Therefore, the change on the apparent AOR could be most probably attributed to a decrease in the fraction of autotrophic organisms in the sludge. The effect of temperature on AOR was not assessed, since all the presented cycles were operated at a similar temperature. Only in the cycle operating in a decreasing DO_{SP} step-wise manner (Fig. 7), the AOR was found to decrease with the decrease of the DO_{SP}, although it could also be related to the decrease in ammonium concentration along the cycle.

Another issue regarding the high variability of the N_2O emissions was the detected N_2O emission peak at the beginning of the aerobic phase in R2-AUT, that can represent up to the 60 % of the total N_2O emitted per cycle. Yu et al. (2010) studied the NO and N_2O emissions in a pure culture of AOB and found high N_2O production linked to transient conditions (from anoxic conditions to aerobic conditions) when NH_4^+ had been accumulated. They concluded that the N_2O production by nitrifying biomass under transient conditions was attributed to a shift in metabolism from low specific activity towards the maximum specific activity (Yu et al., 2010). Therefore, the measured N_2O emission peak at the beginning of the aerobic conditions might be linked to transient conditions, since the aerobic phase of R2-AUT begins after the filling of the reactor with the supernatant of R1-HET reactor, with high NH_4^+ concentration. This peak was not measured in all the cycles and, therefore, it seems to have a dependency on the conditions of the nitrifying biomass before the aerobic phase. Others works have also found an effect of the transient conditions on the N_2O emissions in full-scale WWTPs (Ahn et al., 2010; Ribera-Guardia et al., 2019).

When describing the influence of the DO_{SP} on N_2O emissions, it should be noted that a higher DO_{SP} needs a higher airflow rate in the reactor (Fig. 5B). The average air flowrate increased from 3.35 m^3 h^{-1} (DO_{SP} = 1) to 4.08 m^3 h^{-1} (DO_{SP} = 2) and 4.78 m^3 h^{-1} (DO_{SP} = 3) i.e. 22 % and 43 % higher for 2 and 3 with respect to 1. This aeration flowrate increase favours N_2O stripping and may, at least in a short-term, increase N_2O emissions. The operation of the pilot plant through different DO_{SP}s in R2-AUT revealed the effect of the stripping between liquid and gas phases on the N_2O liquid accumulation and the N_2O measured emission. Fig. 5 shows that when the pilot plant was operated at a low DO (i.e. with low aeration flowrate), the accumulation of N_2O in the liquid increased. This increase could be attributed to the negative effect that decreasing the DO has on N_2O production through the nitrifier denitrification pathway (Massara et al., 2018, 2017; Peng et al., 2015) or to a decrease in the transfer rate between liquid and gas phase (i.e. the N_2O mass transfer coefficient decreased due to a decrease in the air flowrate). Hence, although the N_2O production seems to increase when operating at lower DO, the mass transfer between phase decreases. The accumulated N_2O at the end of the aerobic phase of R2-AUT does not have a negative effect on the overall N_2O emissions of the cycle since, once the aerobic phase of R2-AUT is finished, the supernatant of the reactor is sent to R1-HET to perform the anoxic phase, where N_2O is reduced to N_2.

Therefore, a possible mitigation strategy is to operate at a low DO (down to 1 g O_2 m^{-3}), because less N_2O is emitted due to limited mass transfer rate between phases and the increased accumulation of N_2O will be subsequently denitrified in R1-HET, and not emitted. This strategy shifts the conventional paradigm for mitigating N_2O emissions, as it focusses on preventing N_2O transfer from liquid to the gas phase rather than focusing on N_2O production, since the potential dissolved N_2O would be denitrified in a subsequent step.

Finally, the aeration strategy implemented that emitted less N_2O was operating the plant through intermittent aeration. The results of the intermittent aeration showed a decrease of 40 % on the N_2O-EF of R2-AUT compared to normal operation of the pilot plant (0.40 ± 0.21 % vs. 0.64 ± 0.22 %). A possible explanation is that simultaneous nitrification

and denitrification occurred during the off cycles of the aeration since the denitrifying bacteria can denitrify even in a micro-aerobic environment (Massara et al., 2017). Therefore, the initial peak emissions observed in some experiments (Fig. 5c), attributed to transient conditions, could be mitigated implementing intermittent aeration strategies leading to simultaneous nitrification and denitrification. Rodriguez-Caballero et al. (2015) also proposed a cycle configuration with intermittent aeration to mitigate the N_2O emissions from a full-scale SBR treating municipal wastewater.

5. Conclusions

This study assesses the plant performance and GHG emissions of the mainstream SCEPPHAR novel WRRF configuration at pilot scale and under real environmental conditions and discusses the effect that different aeration strategies have on the N_2O production and emissions. The main findings are:

- Successful removal efficiencies of C, N and P were achieved for a long-term in the pilot plant under shortcut N-removal operating the pilot plant at 8-hour and 12-hour configuration.
- GHG emissions (N_2O and CH_4) showed high variability and were in the low range of typical emission factors measured in conventional full-scale WWTPs, even with high nitrite accumulation, which a priori was unattractive in terms of N_2O emissions.
- Operating the R2-AUT of the pilot plant at different DO_{SP}s did not show a clear trend on the N_2O-EF of the pilot plant, within the DO ranges applied (1 to 3 g O_2 m^{-3}). However, the operation at the lowest value resulted in the lowest N_2O emissions, probably due to the fact that the lower the DO value, the lower the aeration needs and the lower mass transfer from the liquid to the gas. Dissolved N_2O accumulated in the liquid gas and was denitrified in a posterior phase.
- A peak of N_2O emission was found in many cycles of the pilot plant, attributed to the transient conditions of AOB, at the beginning of the aerobic phase of the R2-AUT operation.
- The aeration strategy implemented that most mitigated the N_2O emissions in R2-AUT was the intermittent aeration, reducing the N_2O emissions by 40 % compared to normal operation of the plant.

CRediT authorship contribution statement

Borja Solís was the person in charge of conducting all the analytical work and to write the first draft of the document: formal analysis; methodology; writing – original draft. Albert Guisasola was in charge of the Conceptualization, Data curation, Formal analysis, Supervision, Visualization and review & editing the document. Maite Pijuan was in charge of the Conceptualization, Data curation, Formal analysis & editing the document. Juan Antonio Baeza was in charge of Conceptualization; Data curation; Formal analysis; Funding acquisition; Project administration; Supervision, Visualization and review & editing.

Declaration of competing interest

The authors declare that they have no known competing financial interests or personal relationships that could have appeared to influence the work reported in this paper.

Acknowledgements

Borja Solís is grateful to the PIF scholarship from the Universitat Autònoma de Barcelona. B. Solís, A. Guisasola and J. Baeza are members of the GENOCOV research group (Grup de Recerca Consolidat de la Generalitat de Catalunya, 2017 SGR 1175, www.genocov.com) and M. Pijuan is member of the ICRA-TECH consolidated research group (2017 SGR 1318). This work was funded by the SMART-Plant project (Scale-up of low-carbon footprint Material Recovery Techniques, EUH2020, grant agreement 690323).

Appendix A. Supplementary data

Supplementary data to this article can be found online at https://doi.org/10.1016/j.scitotenv.2022.157626.

References

Ahn, J.H., Kim, S., Park, H., Rahm, B., Pagilla, K., Chandran, K., 2010. N2O emissions from activated sludge processes, 2008–2009: results of a national monitoring survey in the United States. Environ. Sci. Technol. 44, 4505–4511. https://doi.org/10.1021/es903845y.

APHA, 1995. Standard Methods for the Examination of Water and Wastewater. 19th Editi. ed. American Public Health Association, Washington, DC. USA. http://www.standardmethods.org.

Chen, H., Zeng, L., Wang, D., Zhou, Y., Yang, X., 2020. Recent advances in nitrous oxide production and mitigation in wastewater treatment. Water Res. 184, 116168. https://doi.org/10.1016/j.watres.2020.116168.

Cieślik, B., Konieczka, P., 2017. A review of phosphorus recovery methods at various steps of wastewater treatment and sewage sludge management. The concept of "no solid waste generation" and analytical methods. J. Clean. Prod. 142, 1728–1740. https://doi.org/10.1016/j.jclepro.2016.11.116.

Conthe, M., Lycus, P., Arntzen, M.Ø., Ramos da Silva, A., Frostegård, Å., Bakken, L.R., Kleerebezem, R., van Loosdrecht, M.C.M., 2019. Denitrification as an N2O sink. Water Res. 151, 381–387. https://doi.org/10.1016/j.watres.2018.11.087.

Cordell, D., Rosemarin, A., Schröder, J.J., Smit, A.L., 2011. Towards global phosphorus security: a systems framework for phosphorus recovery and reuse options. Chemosphere 84, 747–758. https://doi.org/10.1016/j.chemosphere.2011.02.032.

Daelman, M.R.J., Van Voorthuizen, E.M., Van Dongen, L.G.J.M., Volcke, E.I.P., Van Loosdrecht, M.C.M., 2013. Methane and nitrous oxide emissions from municipal wastewater treatment - results from a long-term study. Water Sci. Technol. 67, 2350–2355. https://doi.org/10.2166/wst.2013.109.

Daelman, M.R.J., van Voorthuizen, E.M., van Dongen, U.G.J.M., Volcke, E.I.P., van Loosdrecht, M.C.M., 2015. Seasonal and diurnal variability of N2O emissions from a full-scale municipal wastewater treatment plant. Sci. Total Environ. 536, 1–11. https://doi.org/10.1016/j.scitotenv.2015.06.122.

EEC Council, 1991. Council directive of 21 may 1991 concerning urban waste water treatment (91/271/EEC). Off. J. Eur. Communities (OJ L 135, 30.5.1991), 40–52. http://data.europa.eu/eli/dir/1991/271/oj.

Gruber, W., Villez, K., Kipf, M., Wunderlin, P., Siegrist, H., Vogt, L., Joss, A., 2020. N2O emission in full-scale wastewater treatment: proposing a refined monitoring strategy. Sci. Total Environ. 699, 134157. https://doi.org/10.1016/j.scitotenv.2019.134157.

Guisasola, A., de Haas, D., Keller, J., Yuan, Z., 2008. Methane formation in sewer systems. Water Res. 42, 1421–1430. https://doi.org/10.1016/j.watres.2007.10.014.

Guo, J.H., Peng, Y.Z., Wang, S.Y., Zheng, Y.N., Huang, H.J., Ge, S.J., 2009. Effective and robust partial nitrification to nitrite by real-time aeration duration control in an SBR treating domestic wastewater. Process Biochem. 44, 979–985. https://doi.org/10.1016/j.procbio.2009.04.022.

Gutierrez, O., Sudarjanto, G., Ren, G., Ganigué, R., Jiang, G., Yuan, Z., 2014. Assessment of pH shock as a method for controlling sulfide and methane formation in pressure main sewer systems. Water Res. 48, 569–578. https://doi.org/10.1016/j.watres.2013.10.021.

IPCC, 2014. In: Pachauri, R.K., Meyer, L.A. (Eds.), Climate Change 2014: Synthesis Report. Contribution of Working Groups I, II and III to the Fifth Assessment Report of the Intergovernmental Panel on Climate Change. IPCC, Geneva, Switze. http://hdl.handle.net/10013/epic.45156.d001.

Jubany, I., Lafuente, J., Baeza, J.a, Carrera, J., 2009. Total and stable washout of nitrite oxidizing bacteria from a nitrifying continuous activated sludge system using automatic control based on Oxygen Uptake Rate measurements. Water Res. 43, 2761–2772. https://doi.org/10.1016/j.watres.2009.03.022.

Kampschreur, M.J., Temmink, H., Kleerebezem, R., Jetten, M.S.M., van Loosdrecht, M.C.M., 2009. Nitrous oxide emission during wastewater treatment. Water Res. 43, 4093–4103. https://doi.org/10.1016/j.watres.2009.03.001.

Kosonen, H., Heinonen, M., Mikola, A., Haimi, H., Mulas, M., Corona, F., Vahala, R., 2016. Nitrous oxide production at a fully covered wastewater treatment plant: results of a long-term online monitoring campaign. Environ. Sci. Technol. 50, 5547–5554. https://doi.org/10.1021/acs.est.5b04466.

Larriba, O., Rovira-Cal, E., Juznic-Zonta, Z., Guisasola, A., Baeza, J.A., 2020. Evaluation of the integration of P recovery, polyhydroxyalkanoate production and short cut nitrogen removal in a mainstream wastewater treatment process. Water Res. 172, 115474. https://doi.org/10.1016/j.watres.2020.115474.

Law, Y., Ye, L., Pan, Y., Yuan, Z., 2012. Nitrous oxide emissions from wastewater treatment processes. Philos. Trans. R. Soc. B Biol. Sci. 367, 1265–1277. https://doi.org/10.1098/rstb.2011.0317.

Mannina, G., Butler, D., Benedetti, L., Deletic, A., Fowdar, H., Fu, G., Kleidorfer, M., McCarthy, D., Steen Mikkelsen, P., Rauch, W., Sweetapple, C., Vezzaro, L., Yuan, Z., Willems, P., 2018. Greenhouse gas emissions from integrated urban drainage systems: where do we stand? J. Hydrol. 559, 307–314. https://doi.org/10.1016/j.jhydrol.2018.02.058.

Marcelino, M., Wallaert, D., Guisasola, A., Baeza, J.A., 2011. A two-sludge system for simultaneous biological C, N and P removal via the nitrite pathway. Water Sci. Technol. 64, 1142. https://doi.org/10.2166/wst.2011.398.

Massara, T.M., Solís, B., Guisasola, A., Katsou, E., Baeza, J.A., 2018. Development of an ASM2d-N2O model to describe nitrous oxide emissions in municipal WWTPs under dynamic conditions. Chem. Eng. J. 335, 185–196. https://doi.org/10.1016/j.cej.2017.10.119.

Massara, T.M.T.M., Malamis, S., Guisasola, A., Baeza, J.A., Noutsopoulos, C., Katsou, E., 2017. A review on nitrous oxide (N2O) emissions during biological nutrient removal from

municipal wastewater and sludge reject water. Sci. Total Environ. 596–597, 106–123. https://doi.org/10.1016/j.scitotenv.2017.03.191.

Mavinic, D.S., Turk, O., 1987. Benefits of using selective inhibition to remove nitrogen from highly nitrogenous wastes. Environ. Technol. Lett. 8, 419–426. https://doi.org/10.1080/09593338709384500.

Mayer, B.K., Baker, L.A., Boyer, T.H., Drechsel, P., Gifford, M., Hanjra, M.A., Parameswaran, P., Stoltzfus, J., Westerhoff, P., Rittmann, B.E., 2016. Total value of phosphorus recovery. Environ. Sci. Technol. 50, 6606–6620. https://doi.org/10.1021/acs.est.6b01239.

Peng, L., Ni, B.J., Ye, L., Yuan, Z., 2015. The combined effect of dissolved oxygen and nitrite on N2O production by ammonia oxidizing bacteria in an enriched nitrifying sludge. Water Res. 73, 29–36. https://doi.org/10.1016/j.watres.2015.01.021.

Remy, C., Jossa, P., 2015. Life cycle assessment of selected processes for P recovery from sewage sludge, sludge liquor, or ash. Deliverable 9.2 of P-REX project. In: Remy, C (Ed.), Sustainable Sewage Sludge Management Fostering Phosphorus Recovery and Energy Efficiency. Kompetenzzentrum Wasser Berlin gGmbH. http://publications.kompetenz-wasser.de/pdf/Remy-2015-821.pdf.

Ribera-Guardia, A., Bosch, L., Corominas, L., Pijuan, M., 2019. Nitrous oxide and methane emissions from a plug-flow full-scale bioreactor and assessment of its carbon footprint. J. Clean. Prod. 212, 162–172. https://doi.org/10.1016/j.jclepro.2018.11.286.

Rodriguez-Caballero, A., Aymerich, I., Marques, R., Poch, M., Pijuan, M., 2015. Minimizing N2O emissions and carbon footprint on a full-scale activated sludge sequencing batch reactor. Water Res. 71, 1–10. https://doi.org/10.1016/j.watres.2014.12.032.

Rodriguez-Caballero, A., Aymerich, I., Poch, M., Pijuan, M., 2014. Evaluation of process conditions triggering emissions of green-house gases from a biological wastewater treatment system. Sci. Total Environ. 493, 384–391. https://doi.org/10.1016/j.scitotenv.2014.06.015.

Vasilaki, V., Massara, T.M., Stanchev, P., Fatone, F., Katsou, E., 2019. A decade of nitrous oxide (N2O) monitoring in full-scale wastewater treatment processes: a critical review. Water Res. 161, 392–412. https://doi.org/10.1016/j.watres.2019.04.022.

Wang, D.-B., Li, X.-M., Yang, Q., Zheng, W., Wu, Y., Zeng, T., Zeng, G., 2012. Improved biological phosphorus removal performance driven by the aerobic/extended-idle regime with propionate as the sole carbon source. Water Res. https://doi.org/10.1016/j.watres.2012.04.036.

Wunderlin, P., Mohn, J., Joss, A., Emmenegger, L., Siegrist, H., 2012. Mechanisms of N_2O production in biological wastewater treatment under nitrifying and denitrifying conditions. Water Res. 46, 1027–1037. https://doi.org/10.1016/j.watres.2011.11.080.

Yu, R., Kampschreur, M.J., van Loosdrecht, M.C.M., Chandran, K., 2010. Mechanisms and specific directionality of autotrophic nitrous oxide and nitric oxide generation during transient anoxia. Environ. Sci. Technol. 44 (4), 1313–1319. https://doi.org/10.1021/es902794a.